

Consequences of dynamically unstable moons in extrasolar systems

Bradley M. S. Hansen,¹^{*},

¹*Mani L. Bhaumik Institute for Theoretical Physics, Department of Physics and Astronomy, University of California, Los Angeles, CA, 90095, USA*

Accepted XXX. Received YYY; in original form ZZZ

ABSTRACT

Moons orbiting rocky exoplanets in compact orbits about other stars experience an accelerated tidal evolution, and can either merge with their parent planet or reach the limit of dynamical instability within a Hubble time. We review the parameter space over which moons become unbound, including the effects of atmospheric tides on the planetary spin. We find that such tides can change the final outcome from merger to escape, albeit over a limited parameter space. We also follow the further evolution of unbound moons, and demonstrate that the overwhelmingly most likely long-term outcome is that the unbound moon returns to collide with its original parent planet. The dust released by such a collision is estimated to reach optical depths $\sim 10^{-3}$, exhibit characteristic temperatures of a few hundred degrees Kelvin, and last for a few thousand years. These properties make such events an attractive model for the emerging class of middle-aged main sequence stars that are observed to show transient clouds of warm dust. Furthermore, a late collision between a planet and a returning moon on a hyperbolic orbit may sterilise an otherwise habitable planet.

Key words: planets and satellites: detection – planets and satellites: dynamical evolution and stability – planets and satellites: terrestrial planets – planet-star interactions – infrared: planetary systems – (stars:) planetary systems⁴

1 INTRODUCTION

The planets of the Solar System are accompanied by a variety of satellites – from the moons and rings of the giant planets to the compact moons of Earth and Mars (Peale 1999). The fact that such structures are relatively common in the Solar system suggests that at least some fraction of the planets formed around other stars must be, in turn, accompanied by their own moons and rings. These satellites also offer insights into the processes that sculpt planetary systems – a subject of great interest at present as observations push our knowledge well past the parameter space occupied by the Solar system planets. Although of great theoretical interest, the low mass ratios and small sizes imply that most exoplanetary moon systems are likely to remain unobservable for some time. Studies of transiting giant planets (Simon et al. 2007; Kipping 2009; Awiphan & Kerins 2013; Lewis 2013; Heller et al. 2014; Hippke 2015; Agol et al. 2015) are now beginning to probe the upper plausible mass range of exomoons (Teachey & Kipping 2018) although it is not clear whether such masses can be explained by traditional processes (Ochiai et al. 2014; Hamers & Portegies Zwart 2018; Hansen 2019; Cilibrasi et al. 2021).

The moons of rocky planets are of particular interest. The formation of compact, low-mass, planetary systems is still a question of active discussion. If the late stages of planetary assembly occur in situ (Hansen & Murray 2012, 2013; Chiang & Laughlin 2013), then moon formation is expected to be a natural consequence of the giant impacts that occur during the final stages of planetary system clearing. On the other hand, if the planets migrate a significant

distance inwards to their current configurations (Ida & Lin 2010; Izidoro et al. 2017), then the additional torques experienced by the system may render systems unstable (Spalding et al. 2016). In this sense, the presence of moons in compact, extrasolar planetary systems may serve as a marker of a late stage of in situ giant impacts. The moons of terrestrial planets may also play a role in preserving planetary habitability. The large lever arm of a moon orbit is potentially a stabilising force against chaotic variations in planetary obliquity caused by resonance between planetary precession frequencies and the secular eigenmodes of planetary systems (Laskar et al. 1993). However, at least in the case of the Earth, it may not be absolutely necessary (Lissauer et al. 2012).

An important consideration in extending the study of satellites to other, compact, planetary systems is that the tidal evolution of moon systems proceeds at a faster pace for planets that are close to their parent stars (Barnes & O’Brien 2002; Sasaki et al. 2012), although this depends somewhat on the parameters of the tidal model (Piro 2018; Tokadjian & Piro 2020). At some level this question is also moot, because terrestrial class planets are themselves difficult to detect, and so the detection of the moons of extrasolar terrestrial in place is still somewhat beyond current capabilities. However, if these systems are short lived, there is the possibility that we may observe the destruction of such objects, and thereby understand something about their frequency of occurrence.

In particular, moons that spiral out to the point at which the circumplanetary orbit becomes unstable will enter an orbit around the star with approximately the same semi-major axis as the parent planet. Although no longer bound to the original planet, they will still be bound to the host star. As such, they will therefore undergo repeated close passages and scatter off the planet. For a moon freed from a

^{*} E-mail: hansen@astro.ucla.edu

massive planet on scales of several AU, this may result in the ejection of the moon from the system. However, for the kinds of compact systems susceptible to tidal evolution, the potential well of the star is too deep for planetary scattering for ejection to be a significant loss channel. As such, nearly all of the freed exomoons will eventually collide with the original host planet and we anticipate a dramatic release of dust would result, and the formation of a temporary infra-red excess around the parent star. Such a scenario may offer an explanation for the class of objects known as EDD (Balog et al. 2009; Melis 2016; Kral et al. 2017; Moór et al. 2021; Melis et al. 2021) hereafter, which are middle aged stars (100 Myr or older) that show infrared excesses well in excess of that expected from the traditional models of planetary system assembly. It is the quantitative aspects of this scenario that we wish to investigate here.

In § 2 we review the evolution of plausible moons in extrasolar rocky planet systems, and examine the expected age range over which they go unstable. In addition to the traditional stellar tides discussed by previous authors (Barnes & O’Brien 2002; Sasaki et al. 2012; Tokadjian & Piro 2020), we also consider the effects of atmospheric tides, which have been postulated (Gold & Soter 1969; Correia & Laskar 2001; Leconte et al. 2015; Cunha et al. 2015; Auclair-Desrotour et al. 2017) to provide asynchronous equilibria around lower mass stellar hosts. In § 3 we discuss the post-ejection evolution of unstable moons, and consider their ultimate fates. In § 4 we discuss the potential observational signatures of such fates.

2 ORBITAL EVOLUTION OF MOONS

The basic picture for a terrestrial-type planet+moon system is that the moon forms as the result of a collision during the late stages of planet assembly. A vapor disk produced in the collision condenses into solid particles at the appropriate Roche radius and these bodies rapidly coalesce into a moon (Stevenson 1987; Canup et al. 2021). The collision also leaves the planet with significant spin and the long-term evolution of the moon is determined by the tidal coupling between the planet and the moon, with three limiting outcomes available (Counselman 1973). If the planet spin is too low, the planet will extract angular momentum from the orbit and the moon will spiral in to merge with the planet. If the planet spin is high enough, angular momentum will be transferred to the moon and it will spiral outwards, eventually to achieve a synchronous rotation or to spiral outwards towards escape. Within the context of a planet orbiting a star, this outwards evolution is truncated when the separation approaches the Hill sphere and the orbit becomes dynamically unstable.

We now know of many planetary systems where the planets are much closer to the host star than the planets in our own Solar system. In such cases, an additional influence must be accounted for. The host star also raises a tide on the planet, and so dissipation of the planetary tide also acts to transfer angular momentum from the spin of the planet to its orbit around the star. This acts to spin the planet down, and so can cause the outwards orbital evolution to reverse, increasing the range of parameter space leading to inspiral. In this scenario, achieving a synchronous state is also unlikely, because synchronism between the planetary spin, planetary orbital frequency and moon orbital frequency would place the synchronous orbit at the approximate location of the Hill sphere.

2.1 Orbital Evolution Equations

There have been several prior calculations of the orbital evolution of moons due to tides (Barnes & O’Brien 2002; Sasaki et al. 2012; Piro

2018; Tokadjian & Piro 2020), and they all give the same qualitative behaviour, but can differ in quantitative ways, primarily because of variations in the assumption of tidal strengths. As in prior works, the orbital evolution of the moon is determined by the gravitational torque acting to transfer angular momentum between the satellite orbit and the planetary spin

$$\frac{d}{dt} \left(M_m (GM_p a_m)^{1/2} + I_m n_m \right) = -N_m \quad (1)$$

where M_m , a_m , I_m and n_m represent the moon mass, semi-major axis, moment of inertia and orbital frequency respectively. The torque N_m is driven by dissipation in the planet and is given by

$$N_m = \frac{3k_2}{2Q} \frac{GM_m^2 R_p^2}{a_m^6} b_m(n_m, \Omega_p) \quad (2)$$

where k_2 and Q are the tidal Love number and quality factor respectively. The function b_m encodes the frequency dependence of the tidal response and will be discussed below.

The orbital evolution of the moon is coupled to the spin evolution of the planet, and so N_m will also act on the spin of the planet. In addition, planets that orbit close to their host stars will also experience a gravitational tide due to the influence of the host star, leading to the operation of a second torque (also driven by dissipation in the planet)

$$N_p = \frac{3k_2}{2Q} \frac{GM_*^2 R_p^2}{a_p^6} b_p(n_p, \Omega_p) \quad (3)$$

where M_* is the mass of the host star and R_p , a_p , n_p are the radius, semi-major axis and orbital frequency for the planet. Similarly, the function b_p encodes the frequency response.

In addition to the gravitational tide, planets with thick atmospheres may experience an atmospheric tide, driven by the heating of the atmosphere by stellar irradiation, and regulated by the forces exerted by the atmosphere on the solid body rotation of the planet. This torque has long been held responsible for the peculiar retrograde spin of Venus in our solar system (Ingersoll & Dobrovolskis 1978; Dobrovolskis & Ingersoll 1980; Correia & Laskar 2001) and may also apply more generally for planets in close orbits (Leconte et al. 2015; Cunha et al. 2015; Auclair-Desrotour et al. 2017). We therefore include an atmospheric torque on the planetary spin

$$N_a = -\frac{3}{2} q_a \frac{3M_* R_p^3}{5\bar{\rho} a_p^3} b_a(n_p, \Omega_p) \quad (4)$$

where $\bar{\rho}$ is the planetary mean density, q_a is the amplitude of pressure field at the base of the planetary atmosphere, and b_a represents the frequency dependence. The sum of the torques N_m , N_p and N_a will determine the evolution of the planetary spin, which will, in turn, drive the orbital evolution of the moon.

One important consideration is the amplitude and frequency dependence of the various torques, which is determined by the physical mechanisms that underlie the dissipation in the planet. For an Earth-like planet, the dissipation is believed to result from the dissipation in the boundary layers of marginal seas (Jeffreys 1921) and resulting from pelagic turbulence (Bell 1975; Egbert & Ray 2000), with a relatively weak frequency response. These dissipation mechanisms require the existence of oceans and dry planets may have weaker dissipation, as estimated for Mars from Lainey et al. (2007). On the other hand, the presence of substantial Hydrogen envelopes observed on many extrasolar planets may enable the propagation of gravity waves, causing dissipation from the conversion of baroclinic waves into barotropic waves on topographic features (Bell 1975;

Balmforth et al. 2002). In the light of the various potential mechanisms, we will adopt a broad parameterisation, calibrated in terms of the tidal Q parameter ($Q_{\oplus} = 30$ serving as a benchmark). We will assume Q is frequency independent, but changes sign with $n_p - \Omega_p$ or $n_m - \Omega_p$. Many previous treatments assume that this occurs as a step function at zero frequency. However, studies of the frequency response of solid bodies (Efroimsky 2012) suggest that, at low enough frequencies, the tidal response is driven by the internal viscosity of the body. As such, we will employ a smoother transition (an arctangent function), parameterised by the viscous timescale of Earth-like planets. For the atmospheric tide model, we adopt the results of Leconte et al. (2015), which are determined from global circulation models under different levels of irradiation and atmospheric pressures. Our default model is for an atmospheric surface pressure of 1 bar, and a level of irradiation appropriate to the inner habitable zone. Appendix A describes the atmospheric torque in quantitative terms and demonstrates the kinds of spin equilibria that can result.

In normalised form, our equation for the evolution of the moon orbit is

$$\frac{dx}{d\tau} = \frac{1}{x^7} (yx^{3/2} - 1) \bar{b}_m \quad (5)$$

where $x = a_m/R_{\oplus}$, $y = \Omega_p/\Omega_k$, $\tau = t/t_0$ and

$$\Omega_k = \left(\frac{GM_{\oplus}}{R_{\oplus}^3} \right) \quad (6)$$

$$t_0 = 0.068 \text{yrs} \frac{Q}{30} \left(\frac{M_m/M_p}{0.0123} \right)^{-1} \left(\frac{M_p}{M_{\oplus}} \right)^{-1/2} \left(\frac{R_p}{R_{\oplus}} \right)^{-5} \quad (7)$$

with α_p is the moment of inertia constant for the planet. The function \bar{b}_m is

$$\bar{b}_m = \frac{2}{\pi} \arctan(\gamma_0(x^{-3/2} - y)) \quad (8)$$

where $\gamma_0 = 10\Omega_k\tau_M = 10^5$ for $\tau_M = 10^{10} \text{s}$ (the characteristic viscous timescale – the Maxwell time). This function ensures a smooth transition from positive to negative torques as the forcing frequency drops below $1/\tau_M$.

Our equation for the evolution of the stellar spin is more complicated, with three different torques contributing.

$$\frac{dy}{d\tau} = \frac{\gamma_1}{x^{15/2}} (yx^{3/2} - 1) \bar{b}_m + \gamma_2 \bar{b}_p + \quad (9)$$

$$\gamma_3 \frac{(y - y_p)}{1 + \gamma_4 (y - y_p)^2} \quad (10)$$

and

$$\gamma_1 = \frac{1}{\alpha_p} \frac{M_m}{M_p} \left(\frac{R_p}{R_{\oplus}} \right)^{-2} \quad (11)$$

$$\gamma_2 = \frac{1}{\alpha_p} \frac{M_*^2}{M_m M_p} \left(\frac{R_{\oplus}}{a_p} \right)^6 \left(\frac{R_p}{R_{\oplus}} \right)^{-2} \quad (12)$$

$$\gamma_3 = \frac{4\pi}{5} \frac{Q\bar{q}_0}{\alpha k_2 \bar{\omega}_0} \frac{M_*}{M_p} \frac{M_{\oplus}}{M_m} \frac{R_{\oplus}}{R_p} \left(\frac{a_p}{R_{\oplus}} \right)^{-3} \quad (13)$$

$$\gamma_4 = 1/\bar{\omega}_0^2 = (\Omega_k/\omega_0)^2 \quad (14)$$

$$\bar{q}_0 = \frac{q_0 R_{\oplus}^4}{GM_{\oplus}^2} \quad (15)$$

$$\bar{b}_p = \frac{2}{\pi} \arctan(\gamma_0(y_p - y)) \quad (16)$$

The quantities q_0 and ω_0 are taken from Leconte et al. (2015).

Moons are assumed to form at just outside the Roche radius (taken to be $x = 3$ here) and the outer limit for dynamical stability is taken to be approximately half of the Hill sphere radius $R_H = a_p(M_p/3M_*)^{1/3}$. This factor is based on numerous prior studies (Domingos et al. 2006; Donnison 2010) and confirmed with our own calculations in § 3. Thus, we truncate our outward evolution because dynamical instability occurs for orbits with or $x > x_i = 119(a_p/1\text{AU})(M_p/M_{\oplus})^{1/3}(M_*/M_{\odot})^{-1/3}$.

2.2 Solutions

Our baseline calculation assumes a replica of the Earth–Moon system, orbiting the Sun at different values of the semi-major axis. The moon evolution begins at $x = 3$, with an initial spin $y = y(0)$, which then evolves according equations (5) and (10). The system is either evolved until the moon spirals in to $x = 3$ again (corresponding to tidal disruption), spirals out to the dynamical instability limit, or reaches a system age of 10^{10} years.

2.2.1 Gravitational Tides only

If we omit the atmospheric tides, our system of equations describes a version of the calculations previously calculated (Barnes & O’Brien 2002; Sasaki et al. 2012; Tokadjian & Piro 2020). The simplest evolution results in the case where the stellar tide is also weak enough to be irrelevant. In that case, the equations have a simple analytic solution – corresponding to basic angular momentum conservation – given by

$$y = y(0) - 2\gamma_1 (x^{1/2} - x(0)^{1/2}). \quad (17)$$

where we assume $x(0) = 3$ here. In the limit $yx^{3/2} \gg 1$, and large $y(0)$, we can also estimate a timescale it will take to spiral out to a particular separation x , namely

$$\tau \sim \frac{2}{13y(0)} x^{13/2} \quad (18)$$

and so we can estimate an outspiral time

$$T_{esc} = 5.4 \times 10^{11} \text{yrs} \left(\frac{a}{1\text{AU}} \right)^{13/2} \left(\frac{0.0123M_{\oplus}}{M_m/M_p} \right) \frac{Q'}{30} \left(\frac{M_p}{M_{\oplus}} \right)^{5/3} \left(\frac{R_p}{R_{\oplus}} \right)^{-5} \left(\frac{M_*}{M_{\odot}} \right)^{-13/6} \left(\frac{y(0)}{0.6} \right)^{-1}. \quad (19)$$

Thus, within the context of the Earth–Moon system, the moon would survive for $a > 0.48\text{AU}$ (in the absence of stellar tides).

The addition of the stellar tides bleeds angular momentum from the system and causes the orbital evolution to reverse if $yx^{3/2} < 1$. Figure 1 shows the nature of the solutions for the gravitational tides only case, for an Earth-like configuration located at three different semi-major axes (1 AU, 0.7 AU and 0.4 AU). The initial spin ($y(0) = 0.6$) and tidal Q ($Q = 30$) were chosen to yield present-day Earth–Moon conditions (the solid point on the right). The equations have been integrated to 10^{10} years, but the solid part of each curve extends only to an age of 4.5 Gyr.

We see that the Earth–Moon system has largely followed the simple solution in which angular momentum conservation is the principal determinant of the orbital properties. At a closer distance of $a=0.7$ AU (approximately the distance of Venus), we see that the stellar tides are capable of spinning the planet down to synchronism with the heliocentric orbit, and that the moon has begun to spiral in and will eventually approach the synchronous orbit, although it will not be tidally disrupted within 10 Gyr. This is the Type II case described by

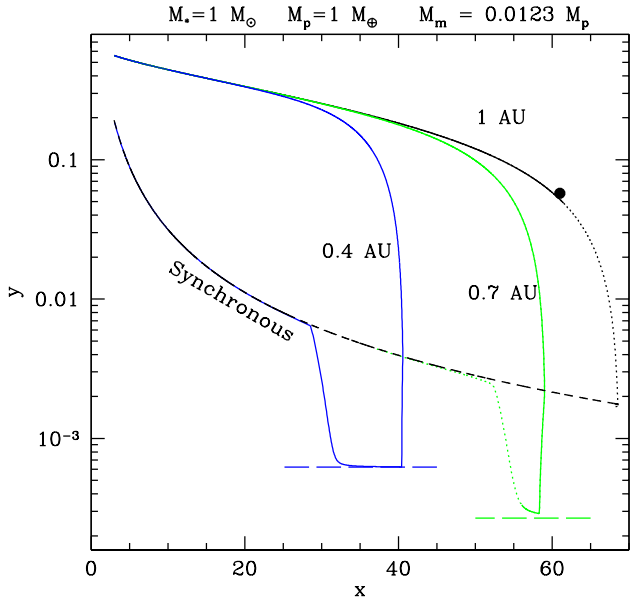


Figure 1. The black, green and blue curves show the evolution of the planetary spin and moon semi-major axis for three systems with the Earth–Moon parameters, but different heliocentric semi-major axes. The solid part of each curve extends up to an age of 4.5 Gyr. The dotted part extends this to 10 Gyr. The short dashed line indicates the locus of spin–orbit synchronism. The horizontal long dashed lines indicate the spin at which the planet is synchronous with its orbital frequency around the Sun (for each case). The solid point indicates the parameters of the present Earth–Moon system.

Sasaki et al. (2012). At an even closer orbit (0.4 AU) we see that the tidal evolution proceeds all the way to inspiral and merger.

2.2.2 Including Atmospheric Tides

The addition of atmospheric tides to the equations changes the spin dynamics of the planet, because the atmospheric tides are of the opposite sign than the corresponding gravitational tide, and allow for the possibility of asynchronous equilibria (Correia & Laskar 2001; Leconte et al. 2015; Cunha et al. 2015; Auclair-Desrotour et al. 2017). Figure 2 shows the consequence of introducing atmospheric tides into the dynamics of the planet+moon system. Once again, we choose masses appropriate to the Terrestrial system, but all curves are calculated at $a = 0.7\text{AU}$.

The dotted curve in Figure 2 shows the locus for $dx/dt = 0$, i.e. the change in orbital evolution from inspiral to outspiral. The solid curve shows the locus of $dy/dt = 0$ for the same equivalent case shown in Figure 1 – $Q=30$ and no atmospheric tides included. The red curve shows the consequence of adding our atmospheric tide model to the system. Although there is no dramatic topological difference, the spin reversal locus is moved to larger x , and this can have important consequences for the system evolution.

An even more dramatic consequence occurs if we increase Q to $Q=100$ (weakening the gravitational tide and therefore enhancing the importance of the atmospheric tide). In this case, the new asynchronous equilibria observed in Leconte et al. (2015) – from which we derived our atmospheric tide model – appear, and are shown by the blue curves. Of particular interest is the branch that appears above

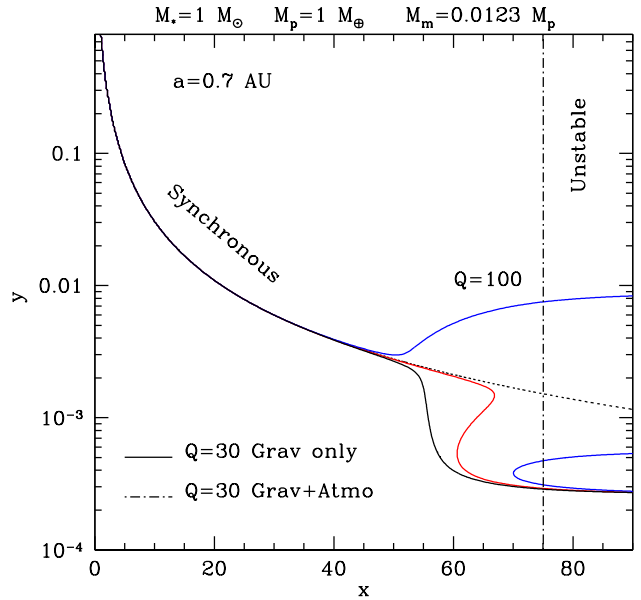


Figure 2. The dotted curve shows the locus for which the sign of the orbital evolution reverses, i.e. $dx/dt = 0$. The solid black curve shows the parameters for which the equivalent spin evolution reverses ($dy/dt = 0$), for the case of $Q=30$ and no atmospheric tides (i.e. the green curve in Figure 1). If we include our atmospheric tide model, we get the solid red curve for $dy/dt = 0$. With the same atmospheric tide but a larger $Q=100$, the sign reversal locus now shows multiple branches (the solid blue curves) corresponding to the appearance of new, asynchronous, spin equilibria. The vertical dot-dashed line shows the edge of the dynamically unstable region.

the synchronous curve. Since the evolutionary curves start at large y and move down as the moon spirals out, they will encounter this sign reversal first, before the reversal in the direction of the orbital motion. As a consequence, the injection of angular momentum into the system by atmospheric tides will refresh the outwards orbital evolution. This is shown in Figure 3, which shows the temporal evolution in each case for the initial conditions used in Figure 1.

The inclusion of the atmospheric tide does indeed refresh the outwards orbital evolution. The action of the atmospheric tide is to weaken the influence of the tidal forces that spin the planet down, and so this means there is more angular momentum available to drive the planet outwards. This effect becomes stronger if the gravitational tide is weaker (Q is larger) but the evolution is slower as well because the timescale depends on Q . This is explored further in Appendix A.

It is important to note that, despite the increased complexity, there are still no globally stable equilibria within the Hill sphere. Even in cases where $dy/dt = 0$ in Figure 2, there are no intersections with the $dx/dt = 0$ curve, so that the orbital evolution of the moon will always pull the system out of (or along) the spin equilibria.

2.3 The influence of tidal strength

The uncertainty in the nature and strength of the tidal forces at play means that there is some uncertainty in the exact outcomes in certain parts of parameter space. To understand the plausible range of variation, we have calculated the evolution of an Earth–Moon analogue system (in terms of mass) for a range of semi-major axis and spin, at both strong ($Q=10$) and weak ($Q=100$) dissipation levels, both

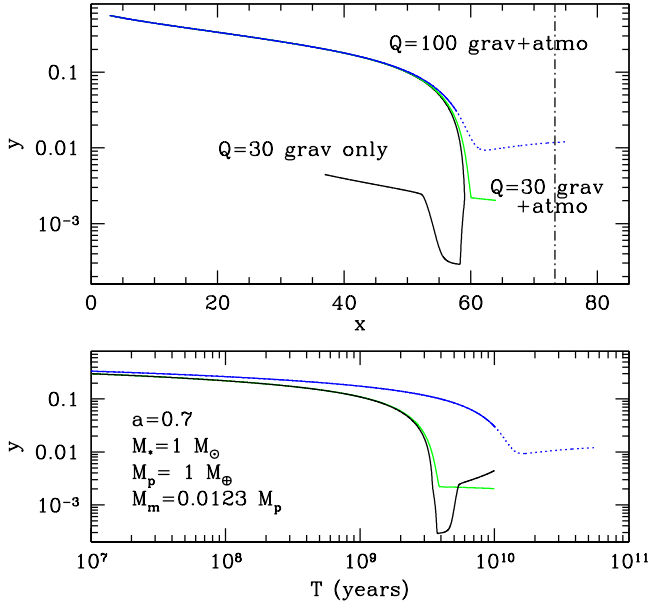


Figure 3. The black curve shows the same evolution as the green curve in Figure 1, with $Q=30$ and no atmospheric tides. In the lower panel we show the temporal evolution of the spin in each case. The green curve in this figure shows the evolution if we keep $Q=30$ but include the atmospheric tide. We see that the character of the evolution is fundamentally changed, as the moon continues to spiral out once atmospheric tides become important. The cyan curve shows the case for which $Q=100$ and atmospheric tides are included. The solid curve extends to 10^{10} years, and the dotted curve extends beyond this. We see that the moon will eventually spiral out to escape, driven by the new, asynchronous equilibrium.

with and without atmospheric torques parameterised in the models of [Leconte et al. \(2015\)](#). Figure 4 shows the resulting distribution of outcomes.

For high enough initial spin, there is sufficient angular momentum for moons to become dynamically unstable for semi-major axes $< 0.7\text{AU}$ (with some dependence on the tidal parameters). For lower values of the spin, the sapping of planetary spin by tides causes inspiral and merger. Inclusion of the atmospheric tide increases the range over which escape is possible, although the effects of atmospheric tides is weaker if gravitational tides are stronger. Furthermore, the variation in the strength of atmospheric tide due to atmospheric pressure (as parameterised in [Leconte et al. \(2015\)](#)) yield small shifts in the boundaries between outcomes, but do not introduce substantial qualitative changes.

2.4 Moon/Planet Mass ratio

The angular momentum balance in a moon–planet system is intimately tied to the mass ratio between the two bodies. Figure 5 shows the effect of varying the moon mass while keeping the planet mass fixed. We show two representative cases, corresponding to the upper left and lower right panels in Figure 4. These represent the two extremes of tidal interaction. The case of $Q=10$ and no atmospheric tides shows systems with efficient tidal interactions, while the case of $Q=100$ and atmospheric tides included represent a less efficient tidal evolution. In this case, all initial spins were set to $y(0) = 0.6$,

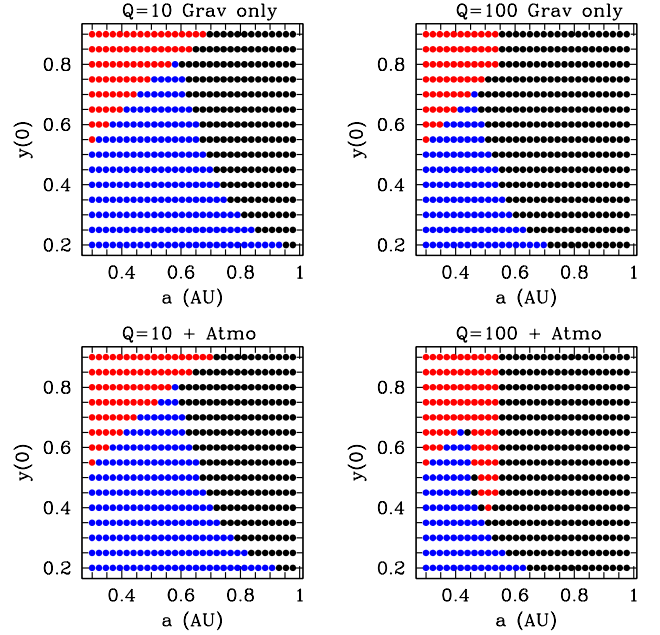


Figure 4. The black points indicate systems where the moon survives for 10 Gyr. The red points indicate systems where the moon spirals out to the point of dynamical instability, while the blue points indicate those systems where the moon ultimately spirals in and is tidally disrupted.

so we probe how the outcomes vary as a function of semi-major axis and moon/planet mass ratio.

We see that dynamical instability occurs only for moon/planet mass ratios similar to those of the terrestrial system. In the case of very massive moons, this is easy to understand, since the initial angular momentum budget in the spin of the planet is fixed for all of these models. There is simply not enough angular momentum to drive a massive moon out to Hill sphere distances, and the planet eventually reaches synchronism and drags the moon inwards. Less intuitively, we find that moons that are too small also move inwards. This results from the fact that small mass moons are very sensitive to changes in the angular momentum budget due to planetary spin-down. As we see from the red curve in the right panel of Figure 5, this evolution initially begins at the shallowest slope of all, but eventually dips down faster as the stellar tides reduce the planetary spin. We see that the moon mass is too small to halt the evolution at the synchronous curve and the spin drops down all the way to the stellar synchronism line, only rising again when the moon spirals in close enough to make its tidal influence significant.

2.5 Planetary Mass Range

The potential observability of the catastrophic destruction of a moon will be enhanced if the moon is larger. Thus, we may ask which combination of plausible parameters yields the largest moons that can escape. We have already seen that we cannot increase the mass of the moon too much, relative to the planet, before the angular momentum required to reach the instability limit becomes prohibitive (§ 2.4). However, we can try to scale up the mass of the planet too.

Although the known planets span several orders of magnitude in mass, our interest here is primarily in rocky planets. The moons of gas giant or Neptune class planets – those with substantial gaseous

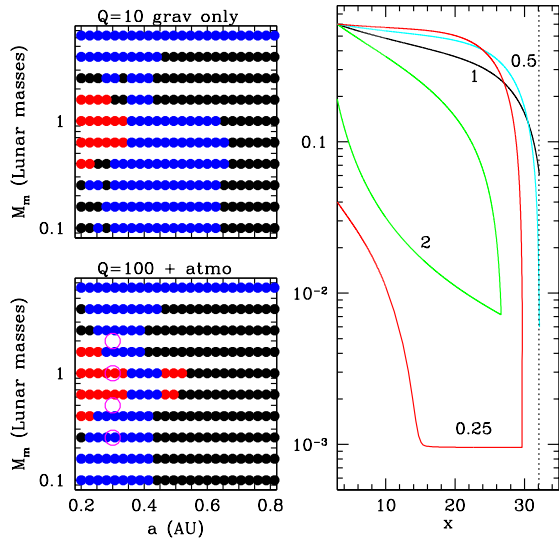


Figure 5. The upper left panel shows the eventual outcome for moons of mass M_m , orbiting a $1M_\oplus$ planet around a $1M_\odot$ star, at the stated semi-major axis. In all cases, the initial planetary spin $\gamma(0) = 0.6$. As before, red represents dynamical instability, blue indicates inspiral and merger, and black represents a moon that survives for 10 Gyr. In this panel, only gravitational tides are included and are parameterised by $Q=10$. In the lower left panel, we show equivalent models except that the gravitational tides are parameterised by $Q = 100$ and atmospheric tides are included. The four open magenta circles represent four models whose evolution is shown in the right hand panel, labelled by the moon mass in Lunar masses. In two cases, the moons reach dynamical instability and in two others, they result in inspiral and merger.

envelopes – may still experience collisions with returning escaped moons, but the impact of a rocky body into a gaseous atmosphere is likely to excavate little debris that will later be observed as a dust population. Instead, we might expect a brief optical flash from the impact, but the bulk of the impact energy is expected to be absorbed by the planet.

It is therefore only for rocky bodies that we expect a significant excavation of debris. The wide variety of exoplanet properties doesn't lend itself to a clear boundary between rocky and non-rocky bodies, with the observed mass-radius distribution suggesting a continuum of Hydrogen mass fractions ranging from negligible to dominant. A significant Hydrogen envelope contribution will also affect the radius, which is the strongest parameter dependence in equation (19). Inspection of the mass-radius relation for known extrasolar planet population (e.g. Weiss & Marcy 2014; Martinez et al. 2019; Swain et al. 2019), restricted to planets with well measured radii and masses, suggests rocky planets can extend up to masses $\sim 10M_\oplus$ and radii $\sim 1.78R_\oplus$.

Thus, we wish to examine the outcomes for moons orbiting massive rocky planets. Figure 6 shows the outcomes for a series of moon systems around a planet with $M_p = 10M_\oplus$ and $R_p = 1.78R_\oplus$, assuming $Q = 100$ and including the atmospheric tide model. We allow the semi-major axis to vary between 0.2–0.8 AU, the moon mass to vary between 1 and 10 Lunar masses, and the initial spin $\gamma(0)$ from 0.2–0.9. Figure 6 shows all cases which result in dynamical instability (red) and in merger (blue)

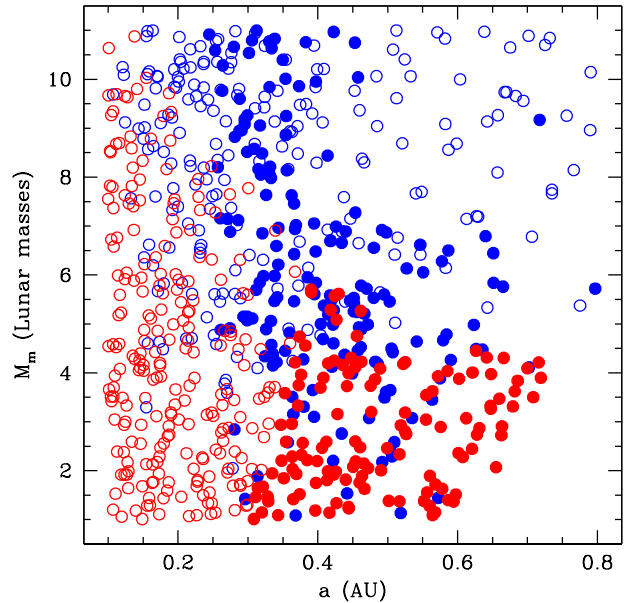


Figure 6. The red points show moons that eventually evolved to the point of dynamical instability, while the blue points evolved to the point of inspiral and merger. All systems orbit a planet of mass $M_p = 10M_\oplus$ and $R_p = 1.78R_\oplus$, that is hosted by a $1M_\odot$ star. Filled circles reach their endpoints at ages > 0.1 Gyr, while open circles end at earlier ages. The density of points gets lower at larger separations, as many of the moons at these distances survive for a Hubble time and are therefore not plotted here.

These results demonstrate that we can get dynamical instability for moons up to ten times the mass of the moon, although these require close-in planets and the moons end their evolution quite quickly. If we also require that the dynamical instability occur at late times (> 100 Myr), then the maximum moon mass is more like $\sim 0.07M_\oplus$.

2.6 Stellar Mass range

The mass of the host star also plays an important role in setting both the Hill radius and the strength of the tide acting on the star. At fixed semi-major axis, a more massive star exerts a stronger gravitational influence and drives tidal and dynamical evolution on a faster timescale. However, lower mass stars are also less luminous, and so the semi-major axis at fixed luminosity (such as would be relevant if one were to track the habitable zone as a function of mass – Kopparapu et al. (2013)) decreases rapidly. The end result is that an Earth-analogue, located in the habitable zone of stars of lower mass than the Sun, must lie closer to the star and the tidal forces lead to an acceleration in their evolution (Piro 2018). Figure 7 demonstrates this for the cases of an approximately Earth-like tidal dissipation ($Q=30$ and no atmospheric tide) and also for a case where the atmospheric tide is important ($Q=100$). In each case, the semi-major axis was chosen to match Earth-like levels of irradiation, given the host star – using the models of Kopparapu et al. (2013).

We see that, for the more massive host stars, the tidal forces are weak enough that the moon can survive for 10 Gyr without disruption. At the lower end of this mass range, the planet does pass through a phase of synchronism with its orbital period, and the moon begins to spiral inwards. For host stars $\sim 0.6M_\odot$, this inspiral is able to proceed

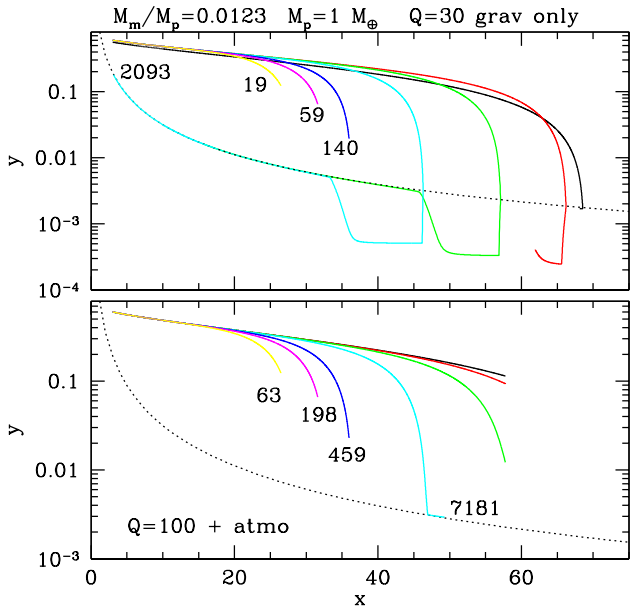


Figure 7. The upper panel shows the evolution of an Earth–moon system located around stars of various mass, with semi-major axes chosen so as to produce the same level of irradiation as the Solar case. The colours correspond to semi-major axes if 1.0 (black), 0.9 (red), 0.8 (green), 0.7 (cyan), 0.6 (blue), 0.5 (magenta) and 0.4 AU (yellow). The dotted line indicates a synchronous moon orbit. For 0.7–1 M_{\odot} , the moon survives to the present day, while it spirals in and merges at 0.6 AU. Interior to this the moon reaches the point of dynamical instability. The system age at merger/instability is listed in Myr. The lower panel is equivalent except that the planetary tidal model now uses $Q=100$ and incorporates atmospheric tides.

to disruption and merger within 2 Gyr. At smaller masses, the moon becomes dynamically unstable before synchronism is reached. This is because the dynamical threshold moves inwards quite rapidly as the host star mass decreases, because the habitable zone distance is a strong function of mass due to the dependance on stellar luminosity. The timescale to instability also decreases as the host star mass decreases.

This distinction in timescale is relevant for the observational identification of mergers or collisions between moons and planets. Planetary systems undergo an extended period of scattering and disruption during the process of clearing out the debris from planetary assembly, and any signature on timescales < 100 Myr are likely to be confused with the production of dust during the standard debris disk clearing stage. However, those systems that take several hundred million years, or more, to complete their evolution will be easily distinguished, as middle-aged stars are not expected to produce significant amounts of dust.

These late-stage events may also be relevant to the habitability of planets themselves. After all, each system in Figure 7 was constructed to have Earth-like gravity and Earth-like temperatures, although changes due to tidal despinning and different host star spectral energy distributions are certainly relevant. Nevertheless, on these timescales > 100 Myr, a planet may have started its biological evolution and taken the first steps towards the construction of an Earth-analogue biosphere. However, tidally induced mergers, or hyperbolic moon collisions (see next section) may provide a late-type catastrophic event that could quench any start in terms of biological evo-

lution. For planets in the habitable zones of these stars, the presence of a moon may eventually wipe life out, instead of preserving it.

3 FINAL EVOLUTION

In § 2 we have reviewed the tidal evolution of the moons orbiting extrasolar rocky planets. As other authors have noted, the tidal evolution of such systems proceeds faster if the planet is located closer to the parent star and many moon systems are not expected to survive to the present day. Some are removed by tidally driven inspiral and disruption, while others spiral out to the point of dynamical instability, at which point they are expected to become unbound with respect to the planet. We have also included, for the first time, the effects of atmospheric tides on the moon evolution. We find that this weakens the tidal evolution in some systems, and can increase the fraction of systems that become dynamically unstable.

Most prior calculations stop at this point, but, if we wish to understand the potential observability of these systems, we must consider what happens to the moons after they become dynamically unstable. Although they are no longer bound to the original host planet, they are still bound to the original host star, and we wish to follow their dynamical evolution beyond the point of instability.

3.1 Dynamical Instability

A moon that reaches the dynamical instability limit will transition to a heliocentric orbit, with a similar semi-major axis as the original host planet. This guarantees close passages with the host planet in the future and the cumulative effect of the gravitational scattering that result will drive orbital evolution. For a more massive planet, with a larger semi-major axis, such a process can eventually eject bodies from the system, or deposit them in the Oort cloud. For a terrestrial class planet, deep in a stellar potential well, the more likely outcome is a planetary collision, with a high probability that it occurs with the original host planet.

To examine the details of this dynamical disruption process, we have integrated the orbits of potentially unstable moons using the direct integration code outlined in Hansen (2019). We begin the moon with circular, coplanar, orbits about the planet with semi-major axes in the range 0.5–0.6 Hill radii, for a planet mass $1M_{\oplus}$, in a 1 AU circular orbit about a Solar mass star. The moon mass is assumed to be negligible, and the orbit is integrated for 1600 years. At this point, the moons are unbound and the resulting heliocentric orbital elements are used to start a direct integration of the heliocentric motion of the test particle moons using the N-body integrator *Mercury* (Chambers 1999). The orbits are then integrated until the test particles are lost, mostly by collision with the planet. A similar calculation of this phase of evolution was performed by Sucerquia et al. (2019), which did find some surviving moons, but the orbital integration lasted only for 0.5 Myr, which is far too short to assess the long-term stability.

3.2 Moon–Planet Collisions

Indeed, all of our ejected moon candidates eventually collide with the original host planet. Most collide within 10 Myr, suggesting that the post-instability evolution is a minor contributor to the total age of the system when the collision occurs. In order to understand the nature of these moon/planet collisions, Figure 8 shows the relative velocity of moon and planet during encounters, as a function of closest distance in each passage (b). We see that most encounters occur at relative velocities below that of the local escape velocity.

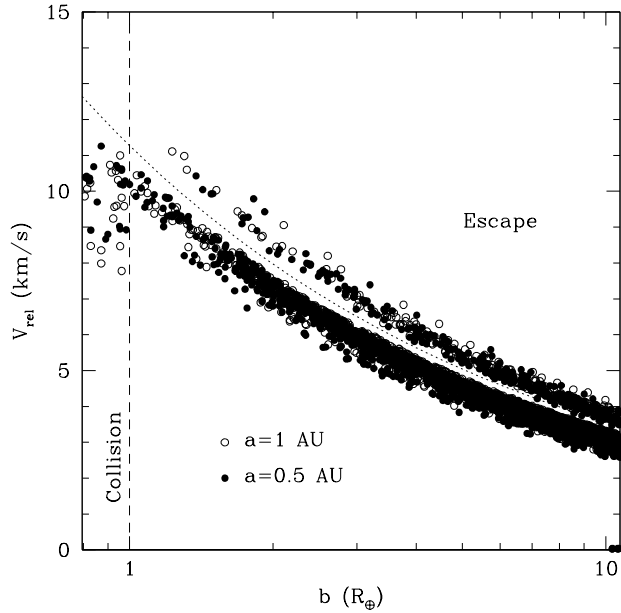


Figure 8. Each point shows the relative velocity of the moon and planet during a post-escape close encounter. The ordinate b is the distance of close approach in each encounter. If $b < 1R_{\oplus}$, then it represents a true physical collision. The dotted curve represents the escape velocity from a $1M_{\oplus}$ mass at distance b . Open circles represent a planet with semi-major axis of 1 AU, while the filled circles show a planet at 0.5 AU. The sample shown here represents 20 realisations of an escaping moon for each case.

This is particularly true for $b < 1R_{\oplus}$, i.e. the terminal close passages that result in a collision. The amount of mass excavated in a collision will be determined by the energy of the impact, and the fact that this is not significantly above escape velocity suggests that the mass released is likely to be less than the original moon mass.

This may, in part, be due to the coincidence that the escape velocity from the surface of Earth is only a factor ~ 3 smaller than the heliocentric orbital velocity (and so comparable to the relative velocity of two bodies with similar semi-major axes). We therefore also show the case where the planet is closer to the star (0.5 AU) in Figure 8. The relative velocity is still dominated by the gravitational focussing due to the planet (as evidence by the fact that the shape of the distribution follows the dotted curve so closely). This is ultimately due to the fact that the moons diffuse out of the instability region, rather than getting a significant ‘kick’, and so their relative velocities with respect to the planet remain quite small, regardless of the semi-major axis. In principle, it might be possible to increase the relative velocities if we reduce the semi-major axis further, but then the lifetime of the moon phase becomes comparable to the lifetime of the original planetary assembly phase and so because hard to distinguish observationally.

3.3 Multiple Planet Systems

The parameters of Figure 8 reflect those of an isolated Earth–mass planet on a circular orbit. Many of the real exoplanet systems contain multiple planets and finite eccentricities. These may, in principle, induce larger relative velocities by introducing larger eccentricities. To examine the effects of this, let us consider an analogue of the Kepler-

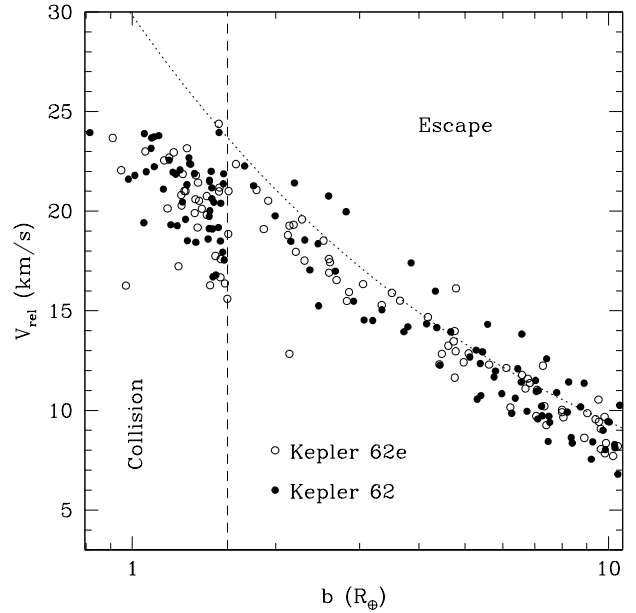


Figure 9. Each point shows the relative velocity of the moon and planet during a post-escape close encounter. The ordinate b is the distance of close approach in each encounter. If $b < 1.7R_{\oplus}$, then it represents a true physical collision. The dotted curve represents the escape velocity from a $7M_{\oplus}$ mass at distance b . Open circles represent a planet with the properties of Kepler-62e orbiting the host star alone. The filled circles show the evolution of the same escaping moons in a system that now contains three planets – Kepler-62d, Kepler-62e and Kepler-62f, with the parameters given in the text.

62 system. Although Kepler has discovered many multi-planet systems, most are too compact for this comparison, as they occur at semi-major axes where the moon evolutionary timescale is too short (see Figure 6). However, Kepler-62e and Kepler-62f have semi-major axes of 0.427 AU and 0.718 AU respectively. We take Kepler-62e to have mass $7M_{\oplus}$ and radius $1.7R_{\oplus}$. In Figure 9 we show the close passage velocities of test particle moons released from Kepler-62e. The open circles represent the case of the single isolated planet, while the filled circles indicate the case where Kepler-62e orbits together with two additional planets, Kepler-62 d (0.120 AU, $10M_{\oplus}$ and $e=0.1$) and Kepler-62 f (0.718 AU, $7M_{\oplus}$ and $e=0.1$). This represents the kind of secular evolution experienced by a compact planetary system.

Figure 9 shows that there is some more spread in velocities in the multi-planet case, but not sufficient to make a qualitative difference in the behaviour of collisions. The lifetimes of the ejected moons are also shorter in the multi-planet system, as the precession induced by the additional contributions to the gravitational potential shorten the intervals between close encounters. Our fundamental conclusion is that almost all moons that are lost through dynamical instability will end up colliding with their original host planet, at velocities of similar order of magnitude to that of the escape velocity from the planet.

3.4 Merger

In cases where the stellar tides come to dominate the evolution, the planet reverses its migration and starts to spiral inwards, spinning the planet up. The eventual outcome of this process is a merger or

tidal disruption. The most likely outcome for this process is tidal disruption, because moons generated by impacts tend to be made of lower density crustal material from the host planet. This disruption may result in the formation of a set of rings (Piro 2018) or a set of smaller moons (Hesselbrock & Minton 2017). Such an episode is likely to be far less dramatic in terms of dust production than the high speed impact associated with a collision.

4 OBSERVABILITY

The essential consequence of the previous sections is that moons formed around rocky planets on scales $\sim 0.4\text{--}0.8$ AU are likely to become dynamically unstable within a Hubble time. When such moons are lost from their parent systems, they are overwhelmingly likely to collide again with their parent planets, on a much shorter timescale than their tidal evolution. Thus, the most likely observational consequence is the event associated with the collision.

Collisions between rocky bodies are expected to produce debris that will collide and grind down to dust, which absorbs and reprocesses stellar light, leading to an infrared excess. This is a generic feature of young planet forming systems, as collisions between rocky bodies are integral part of the planet formation process. However, such excesses become increasingly rare with advancing stellar age, as planetary systems mostly complete their assembly within 100 Myr. Thus, excesses on timescales of Gyr or greater are an indication of some additional processes causing collisions.

Indeed, there are reports of such signatures amongst a subset of older stars (Rhee et al. 2008; Melis 2016; Melis et al. 2021), where excesses of near infrared emission are reported around stars with estimated ages of 100 Myr or more. In order to estimate the size of the infrared excess expected from our model, we note that the impact velocities V_{imp} calculated in Figure 8 and 9 are of order $\sim 70\%$ – 90% of the escape velocities from the surface of the planet. Thus, equating incoming kinetic energy of an impactor of mass M_{imp} with the amount of energy required to unbind an amount of material ΔM from the planet,

$$\frac{1}{2}M_{imp}V_{imp}^2 \sim \alpha_{bind} \frac{GM_p \Delta M}{R_p} \quad (20)$$

we find that

$$\frac{\Delta M}{M_{imp}} \sim \frac{1}{2\alpha_{bind}} \frac{V_{imp}^2 R_p}{GM_p} \quad (21)$$

which is of order unity, since $V_{imp} \sim (GM_p/R_p)^{1/2}$ and $\alpha_{bind} \sim 1/2$. Thus, an impactor like our moon should generate a mass $\sim 0.01M_\oplus$, with possibly even a factor of 10 larger in the case of more massive planet–moon systems.

If this dust is broken into particles of size s , it could, in principle, cover an area

$$A_{IR} \sim 1.7 \times 10^{28} \text{ cm}^2 \left(\frac{M_{dust}}{0.01M_\oplus} \right) \left(\frac{\rho}{3\text{g/cm}^3} \right)^{-1} \left(\frac{s}{10\mu\text{m}} \right)^{-1} \quad (22)$$

which could render a star completely opaque out to semi-major axes $\sim 2\text{AU}$. However, the generation of small dust requires that the debris released from the collision grind down in a collisional cascade, so the amount of dust present in the system at any instant is determined by the rate at which material is ground down.

If the moon debris is initially broken up into pieces with characteristic radius $R \sim 1\text{km}$, then we have approximately

$$N_{rocks} \sim 2.9 \times 10^9 \frac{M_{dust}}{0.01M_\oplus} \left(\frac{R}{1\text{km}} \right)^{-3} \quad (23)$$

each with a mass $\sim 2 \times 10^{16} \text{g} (R/1\text{km})^3$.

We can estimate the collision rate of this debris by assuming they are spread around a torus of semi-major axis comparable to the planetary orbit and thickness comparable to the planetary Hill sphere radius. Relative velocities between dust grains are estimated to be $\sim 10\%$ the local circular velocity. This yields a collision rate

$$\Gamma \sim 3.9 \times 10^{-4} \text{ yr}^{-1} \frac{M_{dust}}{0.01M_\oplus} \frac{1\text{km}}{R} \left(\frac{a}{1\text{AU}} \right)^{-3.5} \left(\frac{M_p}{M_\oplus} \right)^{-2/3} \left(\frac{M_*}{1M_\odot} \right)^{7/6} \quad (24)$$

Note that the collision rate increases as R goes down, so we can assume that the collisional cascade proceeds rapidly to dust size scales. This gives us a rate at which the collisional cascade generates particles of size $s = 10\mu\text{m}$, namely

$$\dot{N} \sim 1.8 \times 10^{30} \text{ yr}^{-1} \left(\frac{M_{dust}}{0.01M_\oplus} \right)^2 \frac{1\text{km}}{R} \left(\frac{1\text{AU}}{a} \right)^{3.5} \left(\frac{M_\oplus}{M_p} \right)^{2/3} \left(\frac{10\mu\text{m}}{s} \right)^3 \quad (25)$$

The amount of dust mass present in the system will be regulated by the processes that remove dust from the system. For dust of size s , in orbit at semi-major axis a around a star of luminosity L , the timescale to spiral inwards due to the Poynting–Robertson effect is

$$T_{PR} \sim 8.4 \times 10^4 \text{ yrs} \left(\frac{a}{1\text{AU}} \right)^2 \frac{s}{10\mu\text{m}} \frac{L_\odot}{L} \quad (26)$$

The dust can also undergo its own collisional evolution and grind down to the point where it is removed by radiation pressure. Following the arguments of Zuckerman & Song (Zuckerman & Song 2012), we derive an even shorter lifetime

$$T_{coll} \sim \frac{1.6 \times 10^{-3}}{\tau} \text{ yrs} \left(\frac{M_p}{M_\oplus} \right)^{1/3} \left(\frac{M_*}{M_\odot} \right)^{-5/6} \left(\frac{a}{1\text{AU}} \right)^{3/2} \quad (27)$$

where τ is the total optical depth of the dust cloud around the star. This estimate follows that of Zuckerman & Song (2012) except that the width of the torus of dust is here assumed to be the Hill radius of the planet, since the dust has a localised origin instead of being generated by a primordial belt of planetesimals.

If we multiply the dust generation rate \dot{N} by the lifetime T_{coll} , we find that the overall optical depth of the dust population generated by this collision is

$$\tau \sim 2 \times 10^{-3} \frac{M_{dust}}{0.01M_\oplus} \left(\frac{R}{1\text{km}} \right)^{-1/2} \left(\frac{a}{1\text{AU}} \right)^{-2} \left(\frac{M_p}{1M_\oplus} \right)^{-1/6} \left(\frac{M_*}{M_\odot} \right)^{1/6} \left(\frac{s}{10\mu\text{m}} \right)^{-1/2} \quad (28)$$

The expected lifetime of the infrared excess can be obtained by estimating the time required to consume the reservoir of N objects created by the collision, assuming the collision rate Γ . This leads to a lifetime

$$T_{IR} \sim 2.4 \times 10^3 \text{ yrs} \left(\frac{M_{dust}}{0.01M_\oplus} \right)^{-1} \frac{R}{1\text{km}} \left(\frac{a}{1\text{AU}} \right)^{3.5} \left(\frac{M_p}{M_\oplus} \right)^{2/3} \left(\frac{M_*}{1M_\odot} \right)^{-7/6} \quad (29)$$

The location of the dust will also determine the temperature of reradiated emission, by virtue of the equilibrium between absorbed and emitted flux

$$T_{dust} \sim 280\text{K} \frac{T_{eff}}{5780\text{K}} \left(\frac{R_*}{R_\odot} \right)^{1/2} \left(\frac{a}{1\text{AU}} \right)^{-1/2} \quad (30)$$

For dust on scales $\sim 0.4\text{--}0.8$ AU around Sun-like stars, temperatures span 300–450 K, falling into the category of ‘Warm dust’.

The age of the system when the moon becomes unstable is a strong function of planetary semi-major axis, and can range from $< 10\text{Myr}$ to $> 1\text{Gyr}$ (see Figure 6 for example). As such, those systems for which the tidal evolution is sufficiently rapid will likely be indistinguishable from a more traditional scenario in which the dust is released by collisions during the actual assembly of the planetary system. However, the age distribution of systems with unbound moon collisions is expected to have a longer tail to Gyr-level ages. To illustrate this, we can estimate the frequency of rocky planetary systems as a function of semi-major axis as $df/da \sim \text{constant}$, based on the empirical observation that the distribution with period is $df/dP \sim P^{-1/3}$ (Youdin 2011). Given the strong dependance of T_{esc} on a (equation 19), we anticipate that the distribution of systems with escape time T should scale as $f(T) \propto T^{-11/13}$, which falls off much slower than the usual exponential that is fitted to the lifetimes of young star infrared excesses.

The features of warm temperatures, large optical depths and potentially ages up to several Gyr make this a natural scenario for the origin of dust observed around older Solar-type stars. The frequency of occurrence of such excesses drops with system age, as expected for a phenomenon associated with the final accumulation of rocky planetary systems. As such, we expect most systems with extreme debris disks to be younger than 100 Myr. Nevertheless, there are a handful of objects which are demonstrably much older, such as BD+20 307 (Rhee et al. 2008; Weinberger et al. 2011), η Corvi (Lisse et al. 2012) or TYC 8830 410 1 (Melis et al. 2021). To estimate the frequency of such objects, we note that the survey of Moór et al. (2021) found an upper limit of 6 candidates out of 78650 sources identified as F5–G9 sources with ages > 100 Myr. This indicates an occurrence rate $\sim 8 \times 10^{-5}$, or a characteristic lifetime $\sim 8 \times 10^3$ years or less. This matches well with the lifetime estimated in equation (29).

These late-time excesses have spurred suggestions of late time asteroid belt collisions, comet disruptions or analogues of the Late Heavy Bombardment. Here we suggest that the tidal evolution, dynamical instability and subsequent collision of the unbound moon offers an alternative scenario that matches the temperatures and optical depths observed for the EDD sample, while also offering a natural explanation of the timescale – a feature lacking from the other scenarios.

5 DISCUSSION

Satellite systems can teach us much about the origins of planets, but are usually well below the detection thresholds of present day astronomical instrumentation. Direct observations are now beginning to probe the most massive satellites orbiting extrasolar giant planets, but direct observation of the moons of terrestrial class exoplanets will probably remain impossible for some time. Nevertheless, indirect observation of moons or the consequences of their presence, may provide some information on this topic. In this spirit we have examined the evolution of moons of rocky exoplanets, subject to both gravitational and atmospheric tides, and also followed this evolution to the ultimate fate of the moon.

(i) As has been shown before, over much of the extant parameter space, the tidal evolution of moons brings them to the point of orbital instability, with the moon becoming unbound from the original host planet and entering a heliocentric orbit about the host star. We have shown that the inclusion of atmospheric tides aids this process by opposing the gravitational torque from the star and

thereby preserving more of the original angular momentum to drive the outward orbital evolution of the moon.

(ii) We have shown that the overwhelmingly most likely outcome of this orbital instability is that the moon will return, in short order, to collide with the original host planet on a near-parabolic orbit. Such impacts are expected to generate a cloud of dust that can lead to an infrared excess. For certain parts of the parameter space, these excesses may occur for ages of several Gyr – much later than expected for the collisions associated with rocky planet assembly – and so should be identifiable on the basis of their unusual time of occurrence.

(iii) Indeed, there is an emerging class of objects, entitled Extreme Debris Disks (EDD) which exhibit all the signatures we associate with these late time, moon–planet collisions. They occur around stars of intermediate to old age, they show dust temperatures which place them within an AU of the host star (so that tides will operate fast enough) and show optical depths $\tau \sim 10^{-4}\text{--}10^{-3}$, consistent with the amount of dust expected from the collision of a moon-sized object. Other scenarios have been proposed to generate the collisions required to explain EDD (Wyatt 2008; Melis 2016; Melis et al. 2021), but all require some level of coincidence to trigger the phenomenon – the onset of a late time dynamical instability (which would require a special set of initial conditions) or the injection of a comet from an external debris belt (which would require another perturber to operate – (e.g. Wyatt et al. 2007)). The moon-based scenario has the distinct advantage of inevitability, in that a moon, once formed, will evolve inexorably according to the angular momentum budget of the system and the strength of the tides operating on it.

(iv) If EDD are the result of collisions of tidally unbound moons with planets, then they attest to the occurrence of moons in extrasolar systems containing rocky planets. Although such moons are a natural occurrence in formation scenarios that include a phase of late stage in situ assembly, they are not guaranteed in scenarios where the planets migrate inwards from more distant locations. This migration is expected to occur during the epoch when the protoplanetary gas disk remains and the torques exerted by the gas disk may render such orbits unstable. The existence of moons in extrasolar planet systems would argue that there was a late stage of planetary collisions in these systems, either due to a genuine episode of in situ assembly (Hansen & Murray 2012, 2013; Chiang & Laughlin 2013) or as the result of the dynamical instability of compact resonant chains (Izidoro et al. 2017).

(v) The presence of the moon in the Terrestrial system is believed to aid the habitability of the Earth by stabilising it against obliquity variations, although some authors suggest the influence is more neutral. However, in those systems which form a moon that later goes dynamically unstable, the formation of moons may point in the completely opposite direction – this may ultimately prove to be harmful for life. The return of an unbound moon on timescales $\sim \text{Gyr}$ means that the planet would experience a catastrophic impact. Such a collision would likely sterilise a planet that had begun to form life in the time it took for the moon to leave and return. Whether life could then start again after this collision is uncertain, especially if such late time collisions remove much of the water from a potentially habitable planet.

Data availability: The data underlying this article will be shared on reasonable request to the corresponding author.

The author appreciates the constructive comments of the referee. This research has made use of the NASA Exoplanet Archive, which is operated by the California Institute of Technology, under contract with the National Aeronautics and Space Administration under the Exoplanet Exploration Program. This research has made use of NASA's Astrophysics Data System, which is operated by the Smithsonian Astrophysical Observatory under NASA Cooperative Agreement 80NSSC21M0056.

REFERENCES

- Agol E., Jansen T., Lacy B., Robinson T. D., Meadows V., 2015, *ApJ*, **812**, 5
- Auclair-Desrotour P., Laskar J., Mathis S., Correia A. C. M., 2017, *A&A*, **603**, A108
- Awiphan S., Kerins E., 2013, *MNRAS*, **432**, 2549
- Balmforth N. J., Ierley G. R., Young W. R., 2002, *Journal of Physical Oceanography*, **32**, 2900
- Balog Z., Kiss L. L., Vinkó J., Rieke G. H., Muzerolle J., Gáspár A., Young E. T., Gorlova N., 2009, *ApJ*, **698**, 1989
- Barnes J. W., O'Brien D. P., 2002, *ApJ*, **575**, 1087
- Bell T. H. J., 1975, *J. Geophys. Res.*, **80**, 320
- Canup R. M., et al., 2021, arXiv e-prints, p. arXiv:2103.02045
- Chambers J. E., 1999, *MNRAS*, **304**, 793
- Chiang E., Laughlin G., 2013, *MNRAS*, **431**, 3444
- Cilibrasi M., Szulágyi J., Grimm S. L., Mayer L., 2021, *MNRAS*, **504**, 5455
- Correia A. C. M., Laskar J., 2001, *Nature*, **411**, 767
- Counselman Charles C. I., 1973, *ApJ*, **180**, 307
- Cunha D., Correia A. C. M., Laskar J., 2015, *International Journal of Astrobiology*, **14**, 233
- Dobrovolskis A. R., Ingersoll A. P., 1980, *Icarus*, **41**, 1
- Domingos R. C., Winter O. C., Yokoyama T., 2006, *MNRAS*, **373**, 1227
- Donnison J. R., 2010, *MNRAS*, **406**, 1918
- Efroimsky M., 2012, *ApJ*, **746**, 150
- Egbert G. D., Ray R. D., 2000, *Nature*, **405**, 775
- Gold T., Soter S., 1969, *Icarus*, **11**, 356
- Hamers A. S., Portegies Zwart S. F., 2018, *ApJ*, **869**, L27
- Hansen B. M. S., 2019, *Science Advances*, **5**, eaaw8665
- Hansen B. M. S., Murray N., 2012, *ApJ*, **751**, 158
- Hansen B. M. S., Murray N., 2013, *ApJ*, **775**, 53
- Heller R., et al., 2014, *Astrobiology*, **14**, 798
- Hesselbrock A. J., Minton D. A., 2017, *Nature Geoscience*, **10**, 266
- Hippke M., 2015, *ApJ*, **806**, 51
- Ida S., Lin D. N. C., 2010, *ApJ*, **719**, 810
- Ingersoll A. P., Dobrovolskis A. R., 1978, *Nature*, **275**, 37
- Izidoro A., Ogihara M., Raymond S. N., Morbidelli A., Pierens A., Bitsch B., Cossou C., Hersant F., 2017, *MNRAS*, **470**, 1750
- Jeffreys H., 1921, *Philosophical Transactions of the Royal Society of London Series A*, **221**, 239
- Kipping D. M., 2009, *MNRAS*, **392**, 181
- Kopparapu R. K., et al., 2013, *ApJ*, **765**, 131
- Kral Q., et al., 2017, *The Astronomical Review*, **13**, 69
- Lainey V., Dehant V., Pätzold M., 2007, *A&A*, **465**, 1075
- Laskar J., Joutel F., Robutel P., 1993, *Nature*, **361**, 615
- Leconte J., Wu H., Menou K., Murray N., 2015, *Science*, **347**, 632
- Lewis K. M., 2013, *MNRAS*, **430**, 1473
- Lissauer J. J., Barnes J. W., Chambers J. E., 2012, *Icarus*, **217**, 77
- Lisse C. M., et al., 2012, *ApJ*, **747**, 93
- Martinez C. F., Cunha K., Ghezzi L., Smith V. V., 2019, *ApJ*, **875**, 29
- Melis C., 2016, in Kastner J. H., Stelzer B., Metchev S. A., eds, Vol. 314, *Young Stars & Planets Near the Sun*. pp 241–246 (arXiv:1509.05726), doi:10.1017/S1743921315006638
- Melis C., Olofsson J., Song I., Sarkis P., Weinberger A. J., Kennedy G., Krume M., 2021, *ApJ*, **923**, 90
- Moór A., et al., 2021, *ApJ*, **910**, 27
- Ochiai H., Nagasawa M., Ida S., 2014, *ApJ*, **790**, 92
- Peale S. J., 1999, *ARA&A*, **37**, 533
- Piro A. L., 2018, *AJ*, **156**, 54
- Rhee J. H., Song I., Zuckerman B., 2008, *ApJ*, **675**, 777
- Sasaki T., Barnes J. W., O'Brien D. P., 2012, *ApJ*, **754**, 51
- Simon A., Szatmáry K., Szabó G. M., 2007, *A&A*, **470**, 727
- Spalding C., Batygin K., Adams F. C., 2016, *ApJ*, **817**, 18
- Stevenson D. J., 1987, *Annual Review of Earth and Planetary Sciences*, **15**, 271
- Sucerquia M., Alvarado-Montes J. A., Zuluaga J. I., Cuello N., Giuppone C., 2019, *MNRAS*, **489**, 2313
- Swain M. R., Estrela R., Sotin C., Roudier G. M., Zellem R. T., 2019, *ApJ*, **881**, 117
- Teachey A., Kipping D. M., 2018, *Science Advances*, **4**, eaav1784
- Tokadjian A., Piro A. L., 2020, *AJ*, **160**, 194
- Weinberger A. J., Becklin E. E., Song I., Zuckerman B., 2011, *ApJ*, **726**, 72
- Weiss L. M., Marcy G. W., 2014, *ApJ*, **783**, L6
- Wyatt M. C., 2008, *ARA&A*, **46**, 339
- Wyatt M. C., Smith R., Greaves J. S., Beichman C. A., Bryden G., Lisse C. M., 2007, *ApJ*, **658**, 569
- Youdin A. N., 2011, *ApJ*, **742**, 38
- Zuckerman B., Song I., 2012, *ApJ*, **758**, 77

APPENDIX A: ATMOSPHERIC TIDE MODEL

The thermal inertia of a planetary atmosphere means that the mass redistribution of the atmosphere, in response to the heating from the central star, lags the true diurnal cycle. This means that the torque, applied by the atmosphere to the planetary interior through boundary layer frictional forces, also lags and contributes an asynchronous contribution to the total torque (Gold & Soter 1969; Correia & Laskar 2001; Leconte et al. 2015; Cunha et al. 2015; Auclair-Desrotour et al. 2017). Although such effects are minor for Earth-like planets, they become progressively more important for planets with high levels of irradiation (and are thought to be the determining factor in the retrograde spin of Venus).

To model atmospheric tides over a broad range of irradiation, we adopt the parameterised model from Leconte et al. (2015). They performed a series of global circulation models to quantify the strength of the atmospheric torque as a function of surface pressure p_s (a proxy for atmospheric mass), composition, and incident stellar flux F_{in} . To these simulations they fit an analytic model which we adopt as function $b_a(n_p, \Omega_p)$ in equation (4), namely

$$b_a(n_p, \Omega_p) = \frac{(\Omega_p - n_p)/\omega_0}{1 + [(\Omega_p - n_p)/\omega_0]^2} \quad (\text{A1})$$

which is parameterised by a characteristic frequency response ω_0 that is a function of p_s , F_{in} and composition. The strength of the atmospheric response is also quantified by an amplitude function q_a (see equation (4)), which is also a function of p_s , F_{in} and composition.

Leconte et al. (2015) provide a table of q_a and ω_0 for a series of different simulations. Our focus is on planets similar to Earth but closer to the Sun, so we adopt the values for $p_s=1$ bar, Earth-like composition, and $F_{in} = 1366W/m^2$. This yields $q_0 = 1180$ Pa and $2\pi/\omega_0 = 32$ days. The atmospheric torque also operates in the opposite direction to the direct gravitational solid-body torque, opening the possibility of an asynchronous equilibrium, as discussed by Leconte et al. (2015). Figure A1 demonstrates how this arises.

The short dashed curve represents the atmospheric torque model above. The long dashed line indicates the equivalent solid body torque, using $\bar{b}_g = \arctan(26.8(y - 1))$ – the numerical value of equation (16) in this case. The red curve indicates the case of $Q = 30$

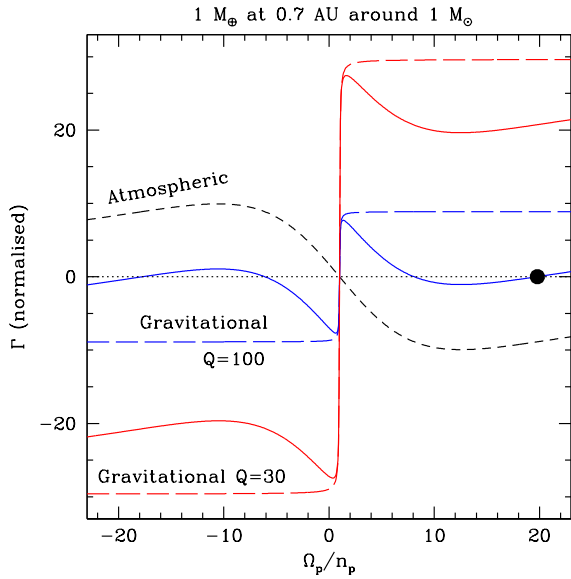


Figure A1. The long-dashed line shows the solid body torque for a $1M_{\oplus}$ planet, orbiting in a circular orbit at 0.7 AU from a $1 M_{\odot}$ star. The red curve is for $Q = 30$ and the blue curve is for $Q = 100$. The short-dashed line is the atmospheric torque operating on the same planet, based on the default model described in the text. The solid line represents the net torque operating on the planet, with the blue and red curves corresponding to the sum of the corresponding solid body torque with the same atmospheric torque. Where these curves cross zero (the dotted line), we have a potential spin equilibrium. The filled solid point indicates the first equilibrium the system would encounter as the planet spins down due to the outspiral of a moon.

and blue indicates the case of $Q = 100$. The solid curves indicate the corresponding net torques in the two cases. The parameter choices for Figure A1 are chosen to represent the same cases as in Figure 2.

The solid black curve in Figure 2 corresponds to the red dashed curve in Figure A1 – the case of no atmospheric torque. The addition of the atmospheric torque to this (resulting in the red solid line) does not change the qualitative nature of the equilibria, but weakens the spin down torque and allows the moon to spiral out further before the planetary spin reverses (as seen in Figure 2). If the solid body torque is weakened (the blue case), then new equilibria appear.

These asynchronous equilibria can have a significant effect on the moon evolution. Shortly after the formation of the moon, the planet is rotating rapidly and will lie off to the right of Figure A1. As the moon spirals out, the planet spins down and moves to the left in the diagram. In the absence of atmospheric tides, this will continue until the planetary spin is synchronous with the orbital frequency, which lies at $\Omega_p/n_p = 1$ in this diagram. However, we see that the system shown in Figure A1 will encounter an asynchronous equilibrium first (shown as a filled circle). As the moon continues to spiral outwards (acting to move the system to the left of the solid point), the atmospheric tides act to spin the planet up and move it back to the stable equilibrium. Thus, the atmospheric tides serve to pump angular momentum into the system, rejuvenating the outward motion of the moon, as is seen in Figure 3.